Thrust Improvement of the Magnetically Enhanced Vacuum Arc Thruster (MVAT)

IEPC-2005-304

Benjamin Tang[*], Luke Idzkowski[†], Michael Au[‡], Don Parks[§], and Mahadevan Krishnan[**]
Alameda Applied Sciences Corporation, San Leandro, CA, 94577, USA

John Ziemer[††]
NASA Jet Propulsion Laboratory, Pasadena, CA, 91109, USA

Abstract: **The Magnetically enhanced Vacuum Arc Thruster (MVAT) is a solid propellant micro-thruster based on a pulsed vacuum arc thruster (VAT) that produces precisely controlled impulse bits. The addition of a co-axial magnetic field to the VAT enhances the thrust efficiency of the thruster and collimates the plasma plume, which reduces contamination of the spacecraft. Alameda Applied Sciences Corporation, along with team member Aerojet, is developing a TRL 5 readiness level MVAT thruster with an integrated Power Processing Unit (PPU). The PPU is an inductive energy store driver that uses the 20V bus voltage to generate both the 1 kV spike needed to trigger the arc as well as the energy to generate the axial magnetic field and the vacuum arc. Since the magnetic field coil is also the primary energy store, there is no mass penalty for the MVAT relative the VAT. This paper presents thrust stand measurements and retarding potential analyses to characterize the improvement of thrust performance with the application of the magnetic field.**

Nomenclature

B =   Magnetic Field
l =   magnetic coil length
I =   Peak current in PPU
N =   Number of turns
r =   radius of magnetic coil
R_p =   Power Processing Unit (PPU) circuit resistance

I.   Introduction

Development of nano-satellites is a strong interest of NASA as well as USAF, DARPA and MDA[1,2,3]. Spacecraft designs are tending towards smaller, less expensive vehicles with distributed functionality. Examples of such platforms include those supported by the University Nano-satellite Program and the Orion Formation Experiment. Distributed satellite networks such as TDRSS, Intelsat, the Global Position System (GPS), Iridium, Globalstar, and

---

[*] Associate Scientist, tang@aasc.net.
[†] Associate Scientist, idzkowski@aasc.et.
[‡] Associate Scientist, mau@aasc.net.
[§] Scientist, parks@aasc.net.
[**] President, krishnan@aasc.net.
[††] Member Technical Staff, Advanced Propulsion Technology Group, john.k.ziermer@jpl.nasa.gov.

the Space Based Infrared Subsystems (SBIRS) already exist. However, while they were designed for a common task, each group of satellites was "non-cooperating." The next wave of constellations will be groups of inexpensive vehicles that interact and cooperate to achieve mission goals. Such nano-satellites can carry small overlapping instruments and offer the benefits of re-configurable, autonomous systems. In such groups, vehicle pointing and positioning will be managed collectively and autonomous vehicles will eliminate the need for extensive ground support. The aim is to replace expensive multi-instrument observatories with low cost, short lead-time spacecraft that can adapt to changing conditions.

To help achieve the nano-satellite concept, the next generation of micro- and nano-thrusters must be capable of a wide range of impulse bits from nN to μN at overall thrust efficiencies of about 10-20%, while maintaining low total system mass (~ 1kg). Scaling existing electric propulsion engines such as Xe ion engines and Hall thrusters down to ~1-10W power levels is not practical. The unavoidable overhead mass of a propellant storage tank, flow controls, and plumbing in Xe ion engines and the needed increase in the magnetic field with decreasing Hall Thruster size renders both types of thrusters less efficient at these power levels.

The Pulsed Plasma Thruster (PPT) has been shown to be a good candidate for many missions requiring ~μN-s to mN-s impulse bits[4]. This type of thruster may be scaled down in current and power to deliver nN-s impulse bits. However, due to the low propellant utilization efficiency (due to late time ablation of the Teflon[TM] insulator) and their requirement for high peak operating voltages (~2 kV), PPTs can at best achieve a thrust efficiency of less than 10%. In addition, the use of a bulky high voltage capacitor in the Power Processing Unit (PPU) considerably reduces their thrust/mass ratio as the overall power and thrust are scaled down. AASC's Vacuum Arc Thruster (VAT), which uses a PPU that employs inductive energy storage, is a low mass alternative that may overcome these limitations and could become the thruster of choice for many micro- and nano-satellite missions.

By adapting the technology of the Vacuum Arc Thruster[5,6,7] and combining it with an external axial magnetic field on the order of 0.05 Tesla, AASC has developed the Magnetically Enhanced Vacuum Arc Thruster (MVAT)[8]. It has been shown to provide up to a 50% higher thrust to power ratio than a conventional vacuum arc thruster. In addition, the applied magnetic field can reduce the width of the plasma plume produced by the thruster and therefore decrease contamination of adjacent optics and sensors on the spacecraft. This paper presents the principle of operation, thrust stand measurements, and preliminary Retarding Potential Analyzer measurements of the MVAT.

II. MVAT Principle of Operation

The MVAT uses an inductive energy storage (IES) approach to drive both the vacuum arc and the axial magnetic field. This results in a Power Processing Unit (PPU) composed of an inductor charged through a semiconductor switch. When the switch is opened, a voltage spike (LdI/dt) is produced which triggers the thruster. The pulse breaks down a carbon-coated insulator (~100 Ω surface resistance), located between the anode and cathode followed by a rapid expulsion of plasma from discrete spots along the insulator. This plasma allows a lower impedance (~10's of mΩ) bulk breakdown in vacuum between the cathode and anode of the thruster. The insulator thus serves only to trigger the arc, carrying a small fraction of the current for ~1 μs or so. . Typical peak arc currents of ~25 A for ~300 to 600 μs are conducted with input bus voltages of 20V. Consequently, most of the magnetic energy stored in the inductor is utilized in the generation of the plasma pulse. The basic design of the inductive energy storage circuit is shown in Fig. 1. The inductor is placed coaxially around the thruster head, thereby having the coil serve as both the driver for the PPU circuit and the source of the axial magnetic field. Thus, energy is stored as the coil is charged as an inductor, and the B-field reaches its maximum value, after which the B-field decays upon release of the stored energy. A photograph of the MVAT head is shown in Fig. 2.
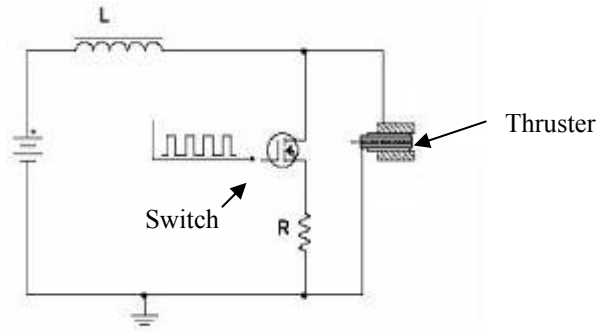
Figure 1. Equivalent circuit for the MVAT PPU.
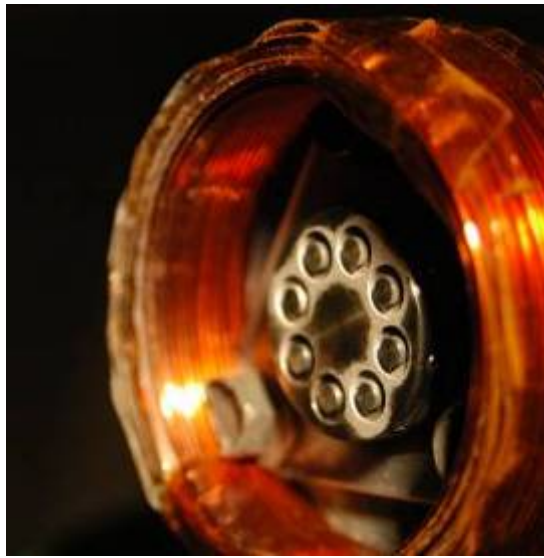
Figure 2. Photograph of the MVAT head assembly.

The main advantage of such a design is the low mass budget of the entire MVAT package (thruster and PPU). Because the coil serves a dual role, there is no need for additional inductors, which would add mass. However, the integration of the PPU driver and the magnetic field source is nontrivial because the currents delivered by the PPU are directly linked to the B-field produced. The B-field generated by the MVAT coil is given by:

$$B = \frac{\alpha \mu_0 N I}{l} \tag{1}$$

where α is a geometrical factor that accounts for the finite solenoid, N is the total number of turns, I is the peak current delivered by the PPU, and l is the length of the coil. The form factor α is given by:

$$\alpha = \sqrt{\frac{1}{(1 + 4(r^2 + l^2))}} \tag{2}$$

where r is the radius of the coil.

The integration of the coil with the PPU introduces the challenge of keeping the total resistance of the circuit small. A large circuit resistance will result in a smaller B-field, a smaller arc current, and limited thrust. The current that runs through the coil and PPU increases as the coil is being charged. Once charged, the peak current in the coil (PPU) is given by Ohm's law:

$$I = \frac{V}{R} \tag{3}$$

where V is the input voltage of 20 V and R is the total resistance of the circuit. Taking the inherent resistance of the PPU and the resistance of the MVAT coil into account, the total resistance is then:

$$R = R_p + 2\pi r \rho N \tag{4}$$

The first term (R_p) takes into account the inherent PPU resistance and the second is the resistance of the B field coil. The radius r of the coil is a mean radius for a multiple layer wound coil and ρ is the resistivity per unit area of the gauge of wire used.

Putting these equations together, we obtain two relationships for the B-field and the current.

$$B = \frac{\alpha \mu_0 V}{l(\dfrac{R_p}{N} + 2\pi r \rho)} \tag{5}$$

$$I = \frac{V}{(R_p + 2\pi r \rho N)} \tag{6}$$

Figure 3 exhibits the results of modeling a 25 mm radius coil with a length of 25 mm. The coil is made of 18-gauge Copper magnet wire. The resulting peak PPU current is also shown. The PPU resistance was experimentally measured at 0.5 Ohms.
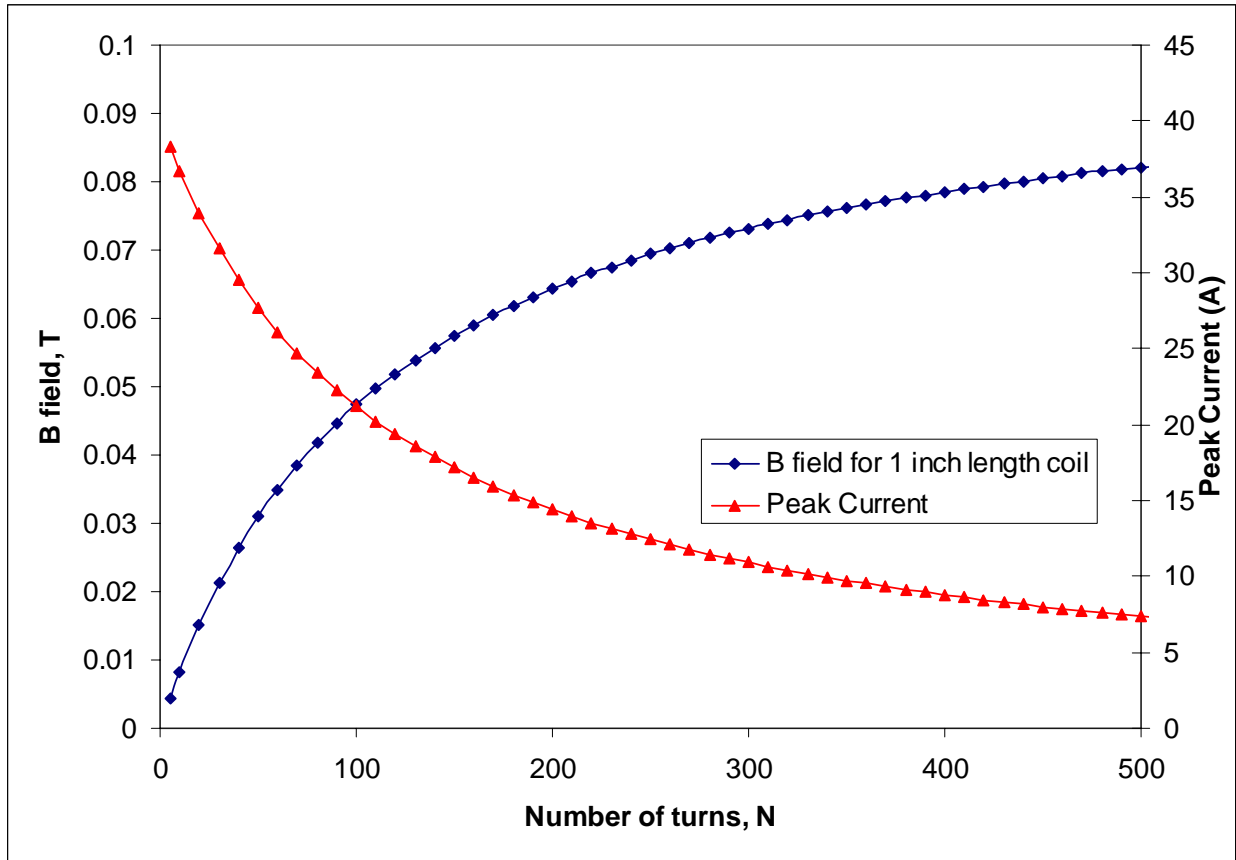
Figure 3. Modeled current and B field as a function of the number of turns using 18-gauge magnet wire.

For the thruster to operate reliably, we have set the minimum peak current to be 20A. This is to ensure a large enough LdI/dt voltage to trigger the thruster when the switch opens. This minimum current also sets the minimum thrust, which, for 50Hz operation, is $\approx$ 125 μN. This peak current is not only that which flows through the PPU after the inductor is charged, but also represents the maximum possible current that can flow through the arc and coil when the thruster fires. As the switch is opened and the thruster fires, the arc current encounters the resistance of the PPU circuit and the added impedance of the plasma plume that is generated. By using 100 turns of 18-gauge wire, we can attain almost 0.05T while having a peak current of 22A (see Fig. 3). Thus, the final mass of the integrated MVAT and PPU is about 1 kg. Although using a 12-gauge wire for the coil would considerably decrease the resistance, the coil's mass would be much higher.

A typical thruster arc current trace, shown in Fig. 4, validates our model. It should be noted that as the thruster discharge current decreases, so does the B-field. This is a consequence of the direct integration of the inductor coil into the PPU. Conveniently, the B-field will cease to exist at the conclusion of every pulse.
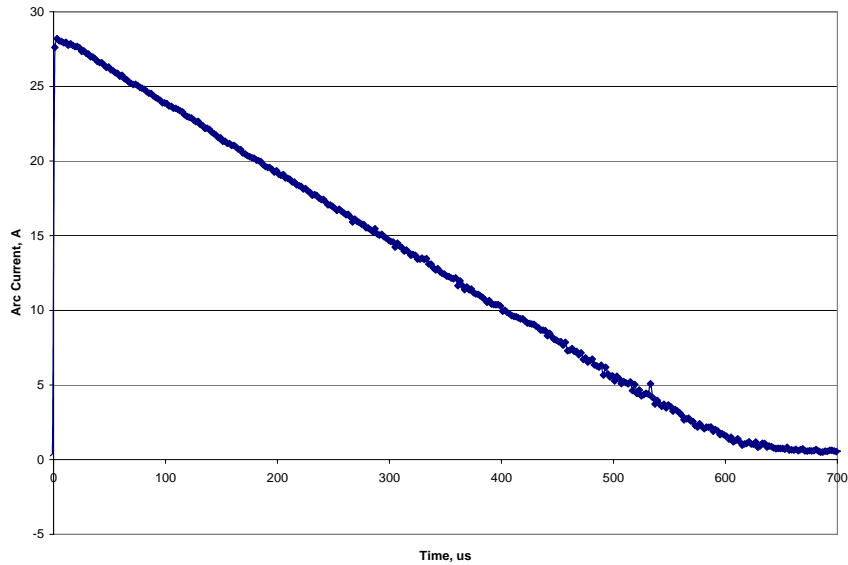
Figure 4. Typical Thruster Arc Discharge current.

The resulting magnetic field profile has also been modeled at the peak current. Figure 5 shows a simulated profile of the magnetic field lines of the coil. As expected, the field lines are more uniform in the interior of the coil than at the front edge. One of the trade offs made in fabricating the coil was the uniformity of the field lines due to the small aspect ratio of the coil. A longer length coil would have produced more uniform field lines to aid in the collimation of the plume, but the magnitude of the B-field (see Eq. 5) would be reduced.

The results of the magnetic field simulation also showed how the field varies with position within the coil. In Fig. 6, two graphs are shown depicting the modeled B field as a function of position along the width of the coil. This
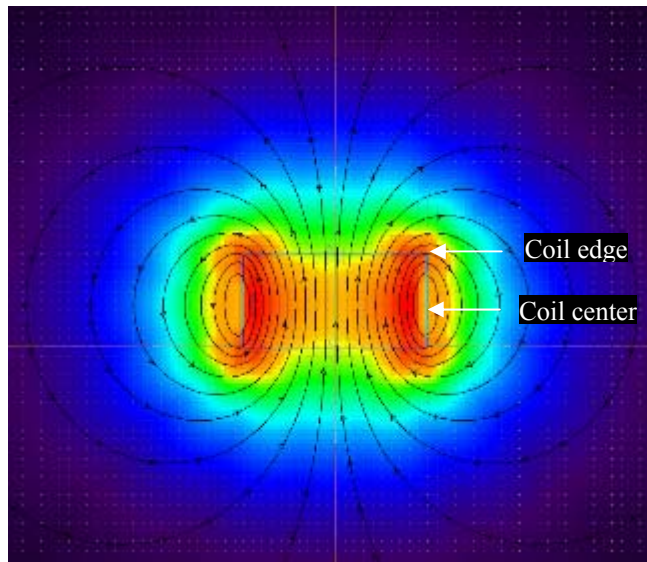
Figure 5. Simulated magnetic field lines of the MVAT coil.

result is important in understanding the tests described in the next section.
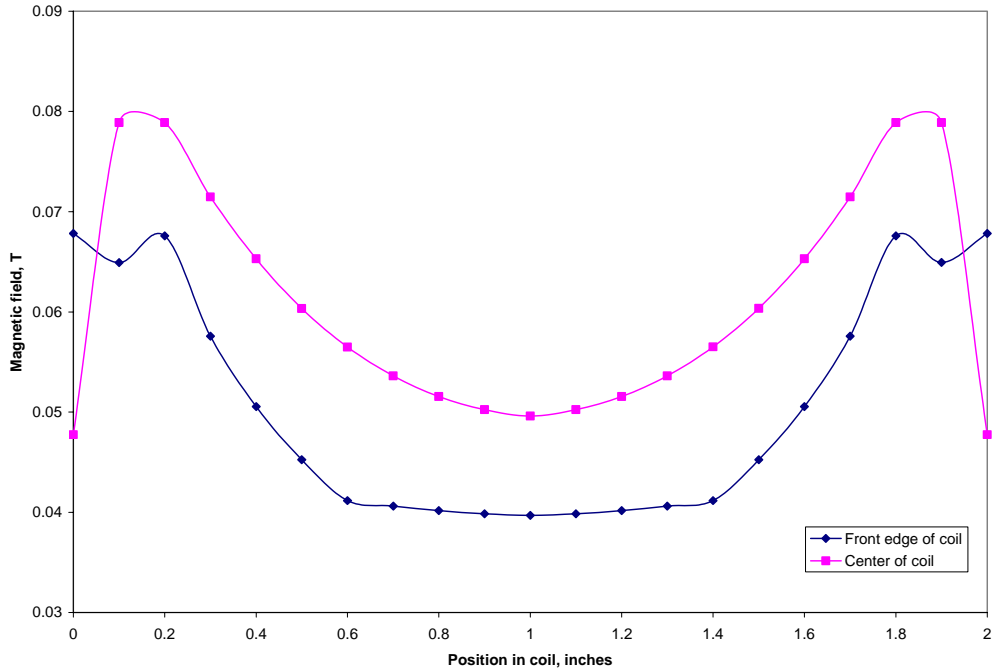
Figure 6. Simulated magnetic field intensity profile as a function of position along the front face and center of the coil.
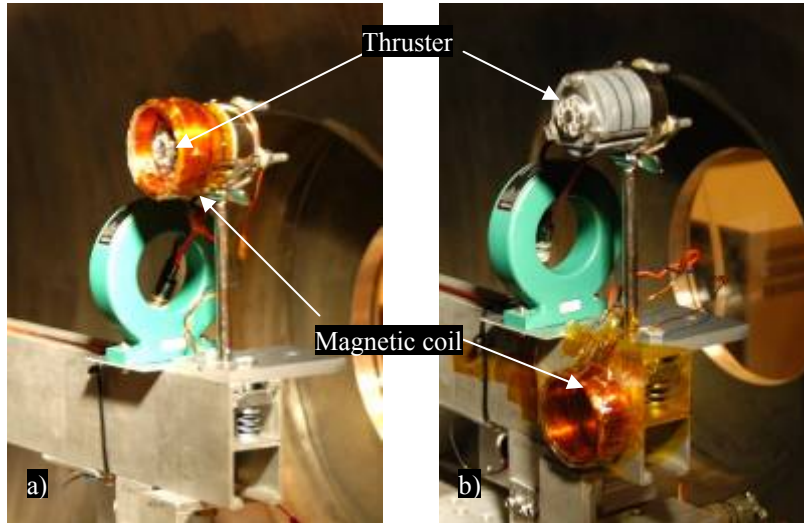
III.   Thrust Stand Measurements

The optimal MVAT thruster configuration was tested on a micro-thrust stand at NASA Jet Propulsion Laboratory to determine the effectiveness of the applied axial magnetic field. The thrust stand apparatus and the measurement procedure are detailed elsewhere[9]. Impulse bits were measured over a burst of 10 shots fired at 50Hz following a standard calibration routine.

To establish a baseline, various measurements were done in which the thruster was mounted parallel and anti-parallel to the thrust stand axis. Orienting the thruster in these two configurations allowed the subsequent thrust measurements to be zeroed as the thrust direction ran parallel to the thrust stand arm. The thrust stand measures only the component of thrust normal to the thrust stand arm. Spurious signals due to vibrations created by firing the thruster could then be subtracted from the thrust measurements. Figure 7 illustrates the orientation of the thruster during the baseline measurements and the actual thrust measurements.
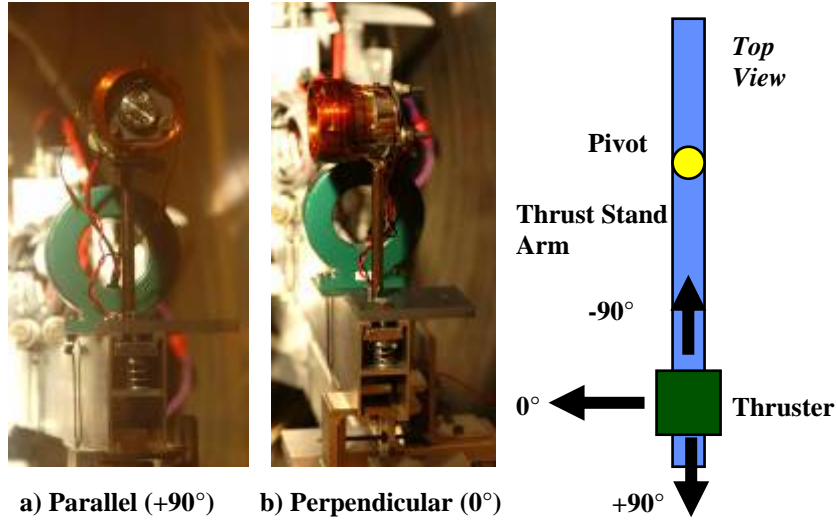
Figure 7. Thrust Stand measurement arrangement: a) Baseline measurement with thruster mounted parallel with the thrust stand axis; b) Thrust measurement with thruster mounted perpendicular to the thrust stand axis.

Following the baseline measurements, the impulse bit (averaged over a burst of 10 shots) of the MVAT was measured in three configurations. The placement of the magnetic coil was changed in each configuration, but the coil remained electrically connected as the inductive storage device for the PPU. Thus, the inductance and resistance of the PPU circuit remained constant. In the first configuration the face of the thruster was centered along the length of the coil. The coil's length is 25 mm and thus the thruster was recessed 13 mm behind the coil edge. The coil was mounted flush with the thruster face in the second configuration. In the final configuration, the coil was removed from the face of the thruster. To keep the system mass constant, the coil was placed on the thrust stand arm. Thus, in this configuration there was no influence of the magnetic field on the plasma plume. The distance of the coil from the thrust stand pivot was also kept identical to the previous two configurations. Configurations 1 and 3 are shown in Fig. 8.

Figure 8. MVAT mounted on the thrust stand in the a) coil centered configuration, and b) coil removed from the thruster head, but still part of the PPU circuit.

The thrust stand measured a finite thrust for the two baseline measurements. The magnitudes of the thrust in the 90º and -90º directions are approximately identical, but in opposite directions. The small difference perhaps is due to interactions of the magnetic field with other components in the vacuum chamber or with the thrust stand itself.
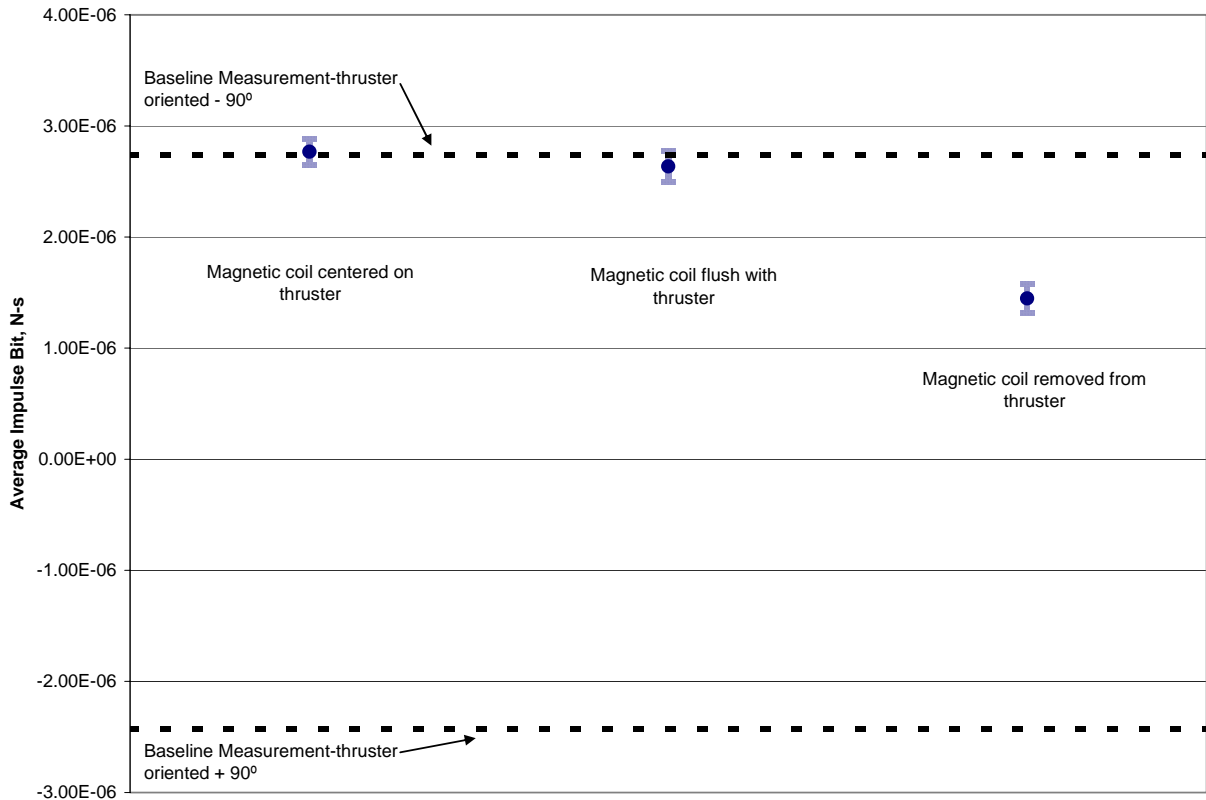
Figure 9. Thrust Stand data with thruster oriented 0º to the thrust stand. The two baseline measurements indicate the thrust measured at + 90º and - 90º.

Because both baseline measurements are similar in value, it is possible that this effect became negligible with the thruster turned 0º. Nevertheless, the data show that there was about a 50% relative improvement in the thrust delivered by the addition of the axial magnetic field. The first configuration, in which the thruster head was positioned in the center of the coil, yielded the maximum thrust due to the strength and uniformity of the field lines at the center of the solenoid. Indeed, Figures 5 and 6 indicate the strength and uniformity of the field lines in this configuration. There was a small decrease in the thrust when the thruster head was mounted flush with the face of the magnetic coil. In this case, the field was slightly lower in magnitude and the field lines were diverging. This is consistent with the results from Anders and Yushkov[10] who found increases in ion velocity and burning voltage with increasing axial magnetic field. It is also possible that the field has a dual effect on the plasma by not only increasing the mean charge state of the ions at the cathode spot, but also more effectively steering or collimating the plume because of their higher charge state.

IV.   Retarding Potential Analysis

The MVAT thruster was also characterized using a Retarding Potential Analyzer. A large RPA was constructed to determine the thrust of the MVAT. The goal is to correlate the impulse bit measured from the thrust stand to the RPA measurements. The RPA has a 125 mm diameter aperture to capture the entire plume of the thruster and is composed of a series of three meshes with a faraday cup of the same diameter.

A polycarbonate body houses each of the 750 line/inch meshes, which have a 55% open area and a wire spacing of about 25 micrometers. The mesh spacing was chosen in consideration of the Debye length of the plasma, which is given by:

$$\lambda_D = (\frac{k_B T}{4\pi n e^2})^{\frac{1}{2}} \tag{7}$$

For a 2 eV plasma of density of 10^{12} cm^{-3}, the Debye length is less than 10 micrometers. This sets the upper limit for the use of such a mesh for the thruster. Placing the series of meshes 15 cm from the thruster ensures that the mesh spacing is comparable to or smaller then the Debye length.

Assuming axial symmetry, an ideal RPA of finite area A whose axis is parallel to the z-axis determines

  (1) instantaneous current through A as a function of time (for a single ion species this is also proportional to dm/dt, where m is the mass of the ions)
  (2) the instantaneous momentum transported through A as function of time, i.e. contribution of A to thrust
  (3) the contribution of A to impulse per pulse.

In particular, if the RPA is sufficiently large and the cross sectional area spans the entire plasma beam, the total thrust and impulse can be determined. If there is no transport of ions 'backward' from the source, a large area detector at large enough z is sufficient to determine the aforementioned quantities.

Consider an axis-symmetric system with cylindrical coordinates r, z where z is the distance from the source plane. The velocity (**v**) distribution function of ions of charge q_i and mass m_i incident on A at the entry position r, z is denoted by $f_i(r, z, \mathbf{v}, t)$. The integral of f_i over the 3-D **v** gives the density n_i at r, z, t. If the ion retarding potential is V the detected current is given by

$$I(A,V,t) = \sum_i q_i \int dA \int_{v_i}^\infty v_z \, f_i(r,z,\vec{v},t) d\vec{v} \tag{8}$$

where v_i is the least axial velocity of an ion that overcomes the potential barrier of the RPA;

$$\frac{1}{2} m_i v_i^2 = q_i V \tag{9}$$

The area integral extends over the entire entrant area A of the RPA. In particular if the RPA intercepts all ions incident on the plane z = constant, then dA = 2πrdr and the integral goes from r = 0 to r = R, the chamber radius. Setting V = 0 gives the total current into the RPA.

Now integrate (8) over all retarding potentials V starting from V = 0 and denote the result by P(A,t);

$$P(A,t) = \int_0^\infty I(A,t)dV = \sum_i m_i \int dA \int_0^\infty v_i dv_i \int_{v_{ii}}^\infty v_z f_i d\vec{v}$$

$$= \sum_i m_i \int dA \int_0^\infty v_z^2 f_i d\vec{v} \tag{10}$$

The last line of (10) follows on changing the order of velocity integrations in the last member of the first line. The final result shows that voltage integration of the current I(A,V, t) gives the rate of momentum transport across the entry plane of the RPA, or the thrust. Integration of P over time (the duration of the pulse) gives the impulse bit.

These results provide the total forward thrust and impulse bit since, by assumption (no loss out radial wall), they do not depend on the z > 0 location of the detector plane. A further assumption is that ions would not reverse their trajectories in a much larger chamber.

The actual measurement involves ramping the potential of Mesh 3 shown in Fig. 10 in a time span of 50 μs while holding Mesh 2 at -100V. A simple RC integration circuit achieved this. Mesh 1 is held floating. R1 is the

measurement resistor at the Faraday cup, which is biased at – 200 V. The spacing between each of the meshes is 64 mm.
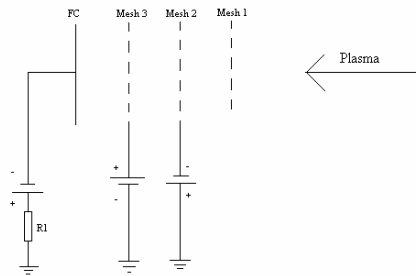
With this configuration, preliminary Faraday Cup current data were taken as a function of various retarding potential ramps. The ramp profiles are shown in Fig. 11 and are labeled by the input voltage, not the actual retarding potential. Figure 12 illustrates the corresponding Faraday Cup current data for each of the retarding potential ramps. These data show a 100 µs window of the FC current taken 100 µs after triggering the thruster. Figure 13 exhibits a full trace of a typical FC current measurement and the time window at which the RPA measurements were taken. Clearly, as the retarding potential reaches about 80V most of the ions have been rejected by the Mesh 3. This test verifies the functionality of our RPA.
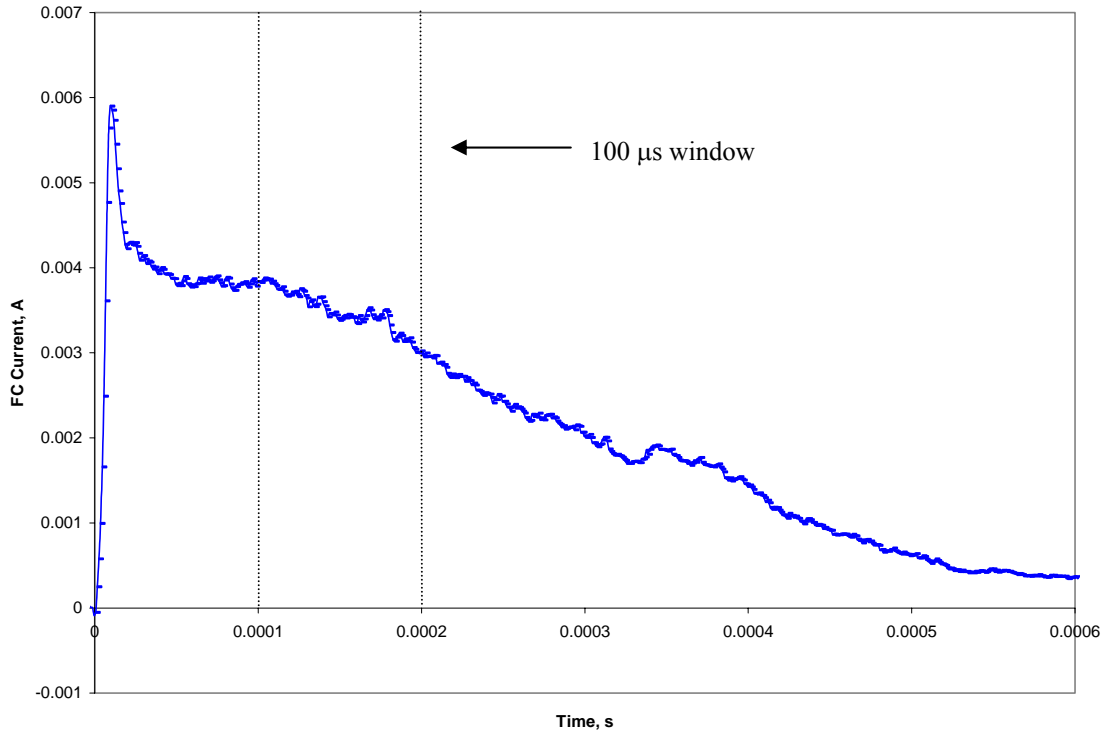

Figure 10.   Schematic drawing of the RPA.
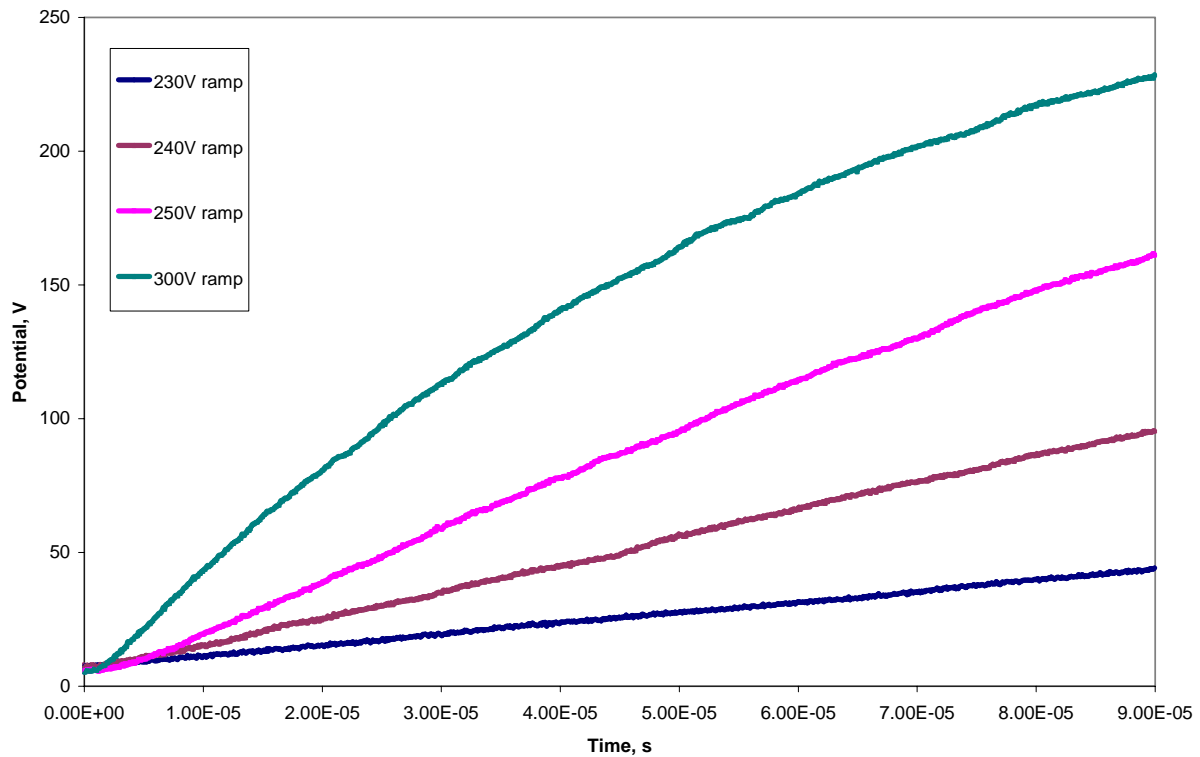
Figure 11.   Ramping retarding potential profiles for RPA measurements.
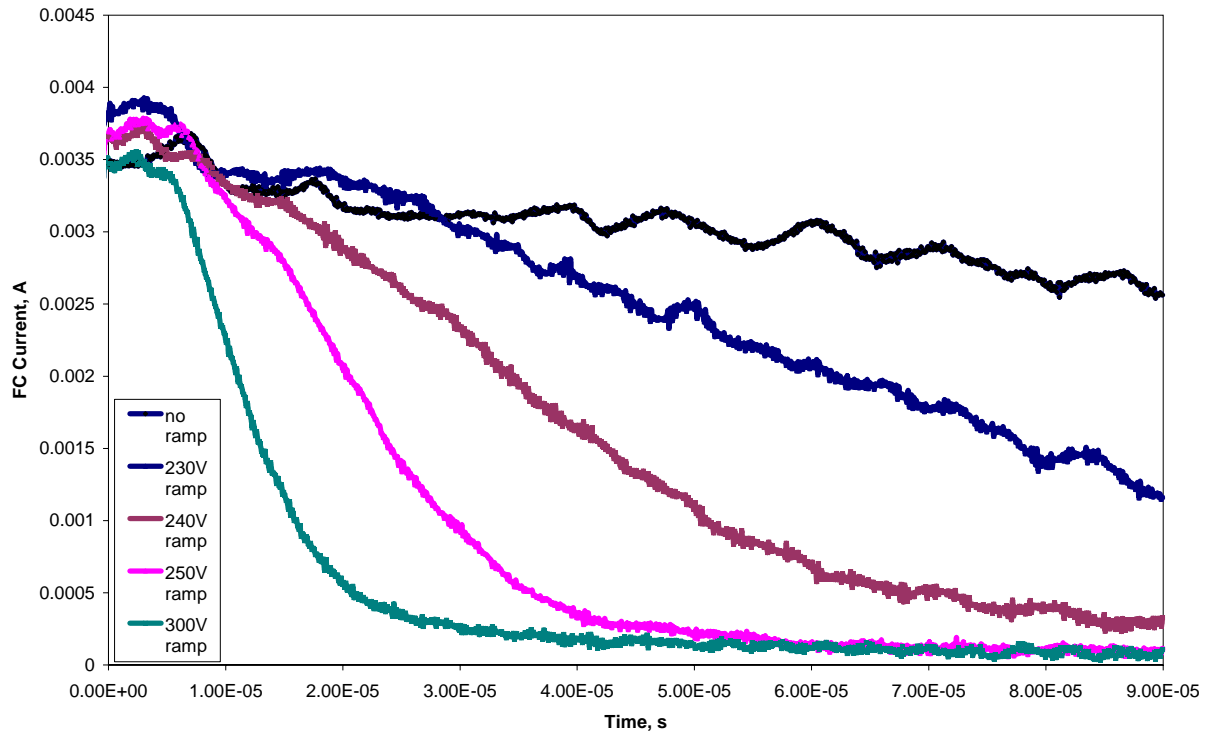
Figure 12.   **Faraday cup currents associated with the ramping voltages in Fig. 11.**

Figure 13.   **Typical Faraday cup current trace.**

V.   Conclusion

We had earlier demonstrated the Vacuum Arc Thruster (VAT) as an efficient alternative to the PPT, providing greater flexibility of propellant and wider operating range at lower voltages. This paper describes an enhancement to the VAT, by adding an axial magnetic field, with *no* additional mass penalty. This happy state is achieved by using the very same inductor that serves as the primary energy store in the inductive store PPU, as also the source of the axial B-field. The MVAT B field coil geometry and configuration have been developed to maximize the B-field and the thrust produced. The prototype MVAT was subsequently tested using JPL's thrust stand and a 50% increase in thrust was generated with the added B-field. RPA measurements, though preliminary, demonstrate its functionality and impulse bit measurements and analyses are pending.

Acknowledgments

References

[1] Birkin, M., Formation Flying and Micro-propulsion Workshop, Lancaster, CA, October 1998.

[2] Dunning, J. and Sankovic, J., 35th Joint Propulsion Conference, Los Angeles, CA, October 1998.

[3] Terster, W., "NASA Considers Switch to Delta 2," *Space News*, Vol. 8, No. 2, 13-19 Jan. 1997, pp., 1, 18.

[4] Birkan, M., AAAF Propulsion Symposium, 2002, 16-355, 2002.

[5] Schein, J., Anders, A., Binder, R., Krishnan, M., Polk, J. E., Qi, N., and Ziemer, J., "Inductive Energy Storage Driven Vacuum Arc Thruster," Review of Scientific Instruments, vol. 72, no. 3, Feb. 2002.

[6] Schein, J., Krishnan, M., Ziemer, J., Polk, J., "Adding a 'Throttle' to a Clustered Vacuum Arc Thruster," AIAA paper, 2002-5716, Nanotech, 2002.

[7] Schein, J., Gerhan, A., Rysanek, F., Krishnan, M., "Vacuum Arc Thruster for Cubesat Propulsion," IEPC-0276, 28th IEPC, 2003.

[8] Keidar, M. and Schein, J., 40th Joint Propulsion Conference, Fort Lauderdale, FL, 2004, AIAA 2004-4117.
[9] Ziemer, J., "Performance Measurements Using a Sub-Micronewton Resolution Thrust Stand," IEPC-238, 27th IEPC, 2001.
[10] Anders, A. and Yushkov, G., J. Appl. Phys., vol. 91, No. 8, 4824 (2002).